

# New Use of Mn-Zn Ferrite Material in Power Electronics Integrated LC Filters

Somo Coulibaly<sup>1</sup>, David Malec<sup>2</sup>, Vincent Bley<sup>2</sup>, Dominique Mary<sup>2</sup>, Benoît Schlegel<sup>2</sup>

<sup>1</sup>DFR-GEE, INP Houphouët Boigny, Yamoussoukro, Côte d'Ivoire

<sup>2</sup>LAPLACE, Université de Toulouse, INPT, CNRS, UPS, Toulouse, France

Email: malec@laplace.univ-tlse.fr

**How to cite this paper:** Coulibaly, S., Malec, D., Bley, V., Mary, D. and Schlegel, B. (2017) New Use of Mn-Zn Ferrite Material in Power Electronics Integrated LC Filters. *Engineering*, 9, 993-1007.  
<https://doi.org/10.4236/eng.2017.912059>

**Received:** October 21, 2017

**Accepted:** December 12, 2017

**Published:** December 25, 2017

Copyright © 2017 by authors and Scientific Research Publishing Inc.  
This work is licensed under the Creative Commons Attribution International License (CC BY 4.0).

<http://creativecommons.org/licenses/by/4.0/>



Open Access

---

## Abstract

A new structure of integrated low-pass LC filter of DC-DC power converter is proposed in this paper. This filter consists in a circular planar coil enclosed between two ferrites substrates. Mn-Zn ferrite has been chosen because of its high permeability and permittivity. In this filter Mn-Zn substrates act not only as a magnetic core but also as a capacitor. In order to reduce the conduction losses in the part of the ferrite used as a capacitor, a particular topology using a blocking layer is proposed. A modelling of the dielectric behaviour of the materials has been performed and injected in a simulation in order to find the resulting LC filter performances and its power range of use. In order to increase the filter efficiency, different solutions have been explored. In particular the inter-turn gap evolution has been optimized to reduce the inter-turn losses. Regarding the bulk losses, BaTiO<sub>3</sub> blocking layers have been added, either upon the ground or the conductor. In this last case a co-firing ferrite tape has been inserted between turns to increase the LC product. Finally the use of low losses Mn-Zn and BaTiO<sub>3</sub> has been proposed and the final characteristics (both electrical and dimensional) of our filter have been compared to conventional ones.

## Keywords

Mn-Zn, BaTiO<sub>3</sub>, LTCC, Power Electronics, LC Filters, Modelling

---

## 1. Introduction

Planar LC passive components, such as inductors and capacitors, have been implemented for many years using a variety of substrates, including standard PC boards, ceramics and silicon. This technology has been only used in low power devices (a few W) with working frequencies ranging up to a few GHz [1] [2] [3].

The filter to be studied in this work is based on this technology but has been designed for higher power and low working frequencies: typically a few kW and a few 10 kHz respectively. In order to reduce the sizes and the weight of this filter, the preliminary structure has been made with only one material acting as both a ferromagnetic and a dielectric. Ferrite material has been chosen to carry out such a filter. Ferrites are indeed one of the best magnetic materials because of their cost, stability and their wide range of technical applications. The Manganese-Zinc (Mn-Zn) ferrites exhibit a suitable high permeability ( $\mu_r$  from 750 to  $2 \times 10^5$ ) but above all a very high permittivity ( $\epsilon_r$  about  $10^4$  at 1 MHz) compared with Nickel-Zinc ones ( $\mu_r$  from 125 to  $2 \times 10^3$  and  $\epsilon_r$  about 25 at 1 MHz respectively). Despite this double property, they are exclusively used as core materials for inductors and transformers [4]-[8]. The limiting factor is their low resistivity (from 1 to  $10 \Omega\cdot\text{m}$ ), justifying that Mn-Zn ferrites have not been already used as capacitors.

The aim of this work is to show how Mn-Zn material may be nevertheless used for both their ferromagnetic and dielectric properties in spite of its low resistivity.

The proposed structure to be studied is a distributed LC filter. A spiral coil is sandwiched between two Mn-Zn substrates. To reduce ineluctable substrate losses, different designs have been proposed and additional materials have been used to obtain a filter having a sufficiently high efficiency. In this paper, only conduction losses occurring in the substrates of the LC filter are estimated; hysteresis and eddy-current associated losses are not taken into account.

In the first part of this paper, the equivalent circuit model per unit volume of Mn-Zn ferrite will be established from dielectric measurements. Starting from fixed geometrical sizes of the studied LC filter, distributed volume and inter-turns capacitors will thus be calculated. Effective inductors will be determined by using a finite-elements method simulation. The resulting LC filter performances (cut-off frequency, slope, filter losses ...) will then be estimated in order to provide useful information to propose a final filter design having sufficiently good performances to be integrated in a power converter. **Figure 1** illustrates a famous DC-DC converter (Buck) that provides a DC voltage (VO) from a DC fixed power supply (VI). VO can be adjusted by controlling the transistor commutation (*i.e.*, the duty cycle). In this simple structure, the LC filter plays an important role in the output voltage ripple value.

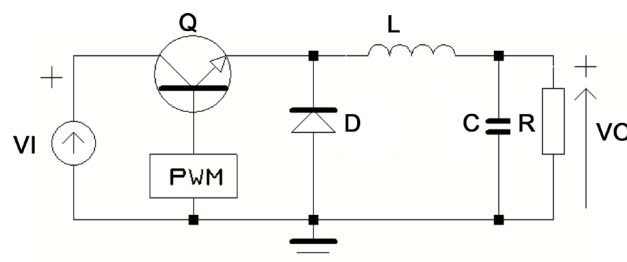


**Figure 1.** Output LC low-pass filter to be used in a Buck converter.

## 2. LC Filter Structure

The structure of the filter consists in a planar spiral coil sandwiched in between two ferrite substrates (Figure 2 & Figure 3). This structure shows both distributed capacitance and inductance between the spiral and the ground planes as shown in Figure 2(a). This structure acts as an electromagnetically integrated LC low-pass filter.

Each element of the equivalent circuit model in Figure 2(b) has to be calculated from both simulations (inductors) and measurements (capacitors).

The spiral coil has been broken into  $2N$ -cells of half circle connected in series. Each half circle contains the equivalent self-inductance, mutual inductances, series resistance and inter-turns impedance. Values of inductances, mutual inductances are obtained by finite-element method. Inter-turn and volume capacitances are calculated from the Mn-Zn ferrite modelling results.

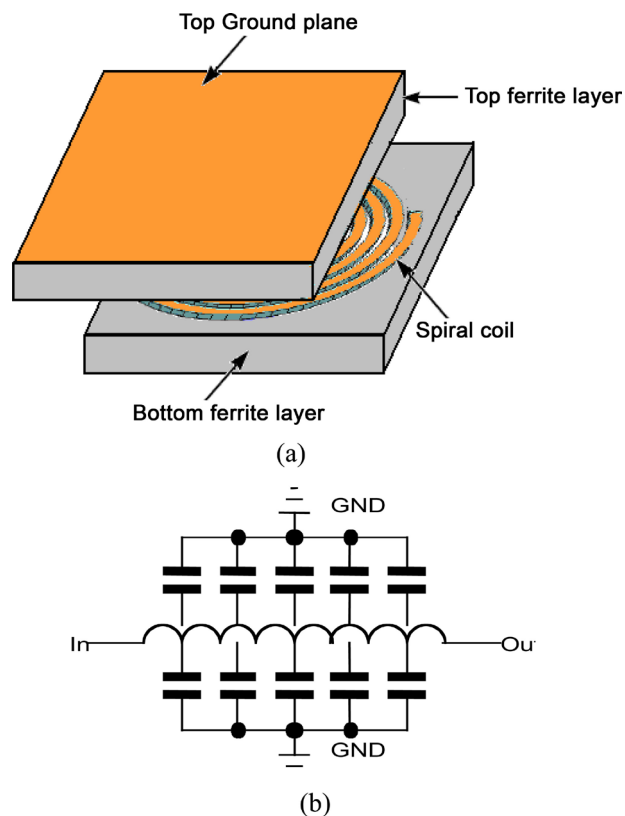


**Figure 2.** (a) Exploded-view of the studied low-pass filter; (b) Equivalent circuit model.



**Figure 3.** Lower Mn-Zn substrate (7 turns).

### 3. Modeling of Mn-Zn Ferrite Dielectric Behavior

The electrical properties of ferrites depend on their polycrystalline structure. The grain and insulating grain boundary are the two main components that determine the variation of resistivity and permittivity [9] [10] [11]. In Mn-Zn ferrites, the grain boundary exhibit different chemical and physical properties from the ferrite grains. The segregation of impurities and partial re-oxidation of  $\text{Fe}^{2+}$  on the grain boundaries during the cooling makes the Mn-Zn ferrite grain boundaries highly insulating in comparison to the grain itself.

These insulating layers are in practice very thin and exhibit a relatively high electrical capacity [9]. The structure and the usual equivalent circuit are shown in **Figure 4(a)** and **Figure 4(b)** [9] [11].  $R_g$  and  $R_{gb}$  are the grain and the grain boundary resistances respectively.

The equivalent circuit model of **Figure 2(b)** has been used for the modelling of the dielectric behaviour of Mn-Zn commercial ferrites (3F3 FERROXCUBE) whose relevant characteristics are summarized in **Table 1**.

In order to extract the values of the three components of **Figure 4**, measurements have been carried out using a HP4284A RLC-meter. Samples to be measured were composed of a 3.5 mm-thick Mn-Zn samples with two gold deposited

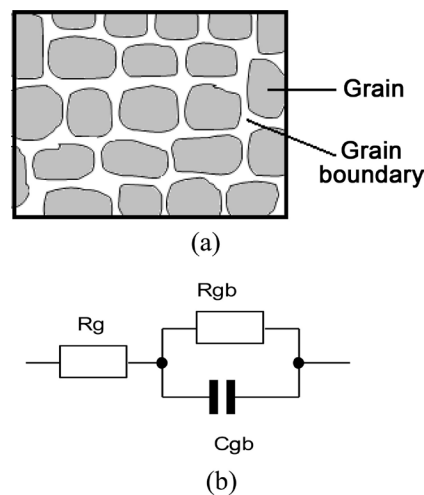


**Figure 4.** (a) Physical polycrystalline structure; (b) Equivalent circuit model.

**Table 1.** Main characteristics of 3F3-power ferrite under study.

PARAMETERS	VALUES
Grain size	5 $\mu\text{m}$
$T_c$	>200°C
$\mu_r$ (T = 25°C)	1800
$\mu_r$ (T = 100°C)	2600
$B_s$ (T = 25°C)	440 mT
$B_s$ (T = 100°C)	370 mT
Frequency	Up to 500 kHz

electrodes (diameter: 10 mm). A good fitting has been obtained between simulated and experimental frequency response of the ferrite (in the frequency range of 10 Hz - 1 MHz). Results obtained at  $T = 20^\circ\text{C}$  have been reported in **Table 2**. From the value of  $C_{gb}$ ,  $\epsilon_r$  has been estimated to be about  $6.5 \times 10^4$ .

It should be noted that the dielectric equivalent circuit model of other Mn-Zn ferrites (*i.e.*, doped ferrites) may be different from this model. Indeed, a highly resistive layer may be present on the surface of Mn-Zn grains; these resistive layers may be fitted by a supplementary RC-cell [10].

As Mn-Zn has a sufficiently high relative permittivity, fringing effect can be neglected [12]. Consequently, the results obtained from the equivalent circuit model can thus be directly used to calculate the corresponding capacitances of the studied filter.

## 4. Filter Circuit Model

### 4.1. Filter Model

The spiral inductor in between the ferrite substrates is circular. Since the spiral inductor is a distributed structure, our proposed model is based on a distributed model. Several works have already shown that a turn may be represented by a lumped model as reported in **Figure 5** [13]. In order to get a better accuracy, the spiral of  $n$ -turns has been broken into  $2n$ -half-turns. Thus, each half-turn represents the lumped model of **Figure 5**. This choice has already been preferred because in some of our studied LC filter designs the inter-turns distances vary from the input to the output filter.

The overall model consists in  $2n$ -circuits connected in series to form a distributed model. The inter-turns impedances between adjacent turns are to be considered, especially by using a high permittivity substrate. They are distributed at the front and the end of the inter-turns, leading to  $2(n - 1)$  inter-turns impedances. To illustrate the principle of this modelling, let us consider a LC filter with 2 turns of **Figure 6(a)**. Index 1 and 2 correspond to the first half turn, 3 and 4 to the second half turn, and so on. The resulting filter circuit model is

**Table 2.** Fitting parameters of Mn-Zn AT  $T = 20^\circ\text{C}$  (frequency range: 10 Hz - 1 MHz).

$R_g$ ( $\Omega$ )	$R_{gb}$ ( $\Omega$ )	$C_{gb}$ (nF)
66	13	16

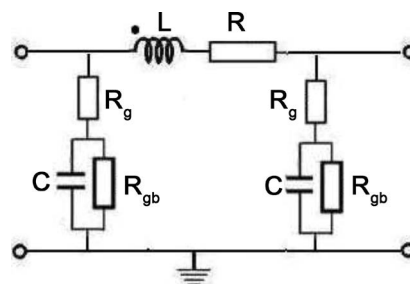
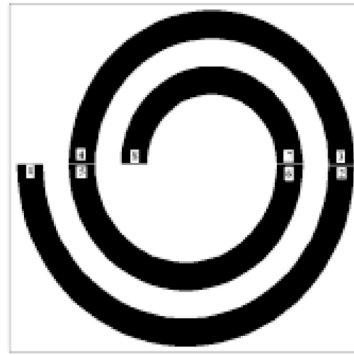
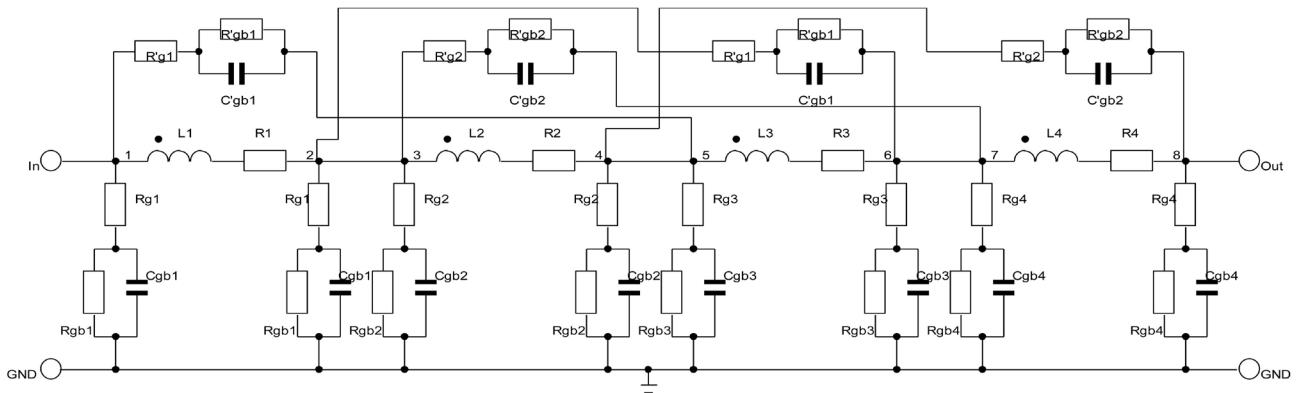


**Figure 5.** Half-turn lumped model.



(a)



(b)

Figure 6. 2-turns filter (a) and its associated circuit model (b).

done in **Figure 6(b)**. Index 1 to 8 of **Figure 6(a)** may be found in **Figure 6(b)**. Since the Mn-Zn substrate presents a high permittivity, we did not take into account the capacitor corresponding to the air gap between two neighbouring half-turns. Consequently, inter-turns capacitors of **Figure 6** are only those due to the Mn-Zn substrate.

#### 4.2. Model Parameters Determination

##### Inductances

Instead of using any analytical formula to calculate both self and mutual inductances, finite-elements method (FEMLAB [14]) has been used to obtain these values. The simulation was performed using a 2D-axisymmetric assumption. Self-inductances ( $L_{si}$ ), positive and negative mutual inductances ( $M_{ij}^+$  and  $M_{ij}^-$  corresponding to positive and negative interactions between all half-turns) have been estimated by successive simulations to obtain the total inductance  $L_i$  as in Equation (1).

$$L_i = L_{si} + \sum M_{ij}^+ - \sum M_{ij}^- \quad (1)$$

Note that in this model, the inductances are assumed to be constant over the frequency range of interest.

### Coil resistances

The resistances of each half-turn have been estimated by using the classical relationship as in Equation (2).

$$R = \rho \cdot \frac{l}{S} \quad (2)$$

where  $\rho$  is conductor resistivity (here copper),  $l$  and  $S$  are conductor length and cross-sectional area respectively. In the forthcoming LC studied structures, the sizes of the coil conductor will be chosen to avoid any skin effect.

### Substrate impedances

Both resistances and capacitances of the ferrite substrates are calculated by using the fitting parameters of **Table 2**. The parameters  $R_{g2}$ ,  $R_{gb2}$  and  $C_{gb2}$  of the filter impedance are related to those of the tested sample ( $R_{g1}$ ,  $R_{gb1}$  and  $C_{gb1}$ ) by the following equations:

$$\begin{cases} R_{g2} = K_R \cdot R_{g1} \\ R_{gb2} = K_R \cdot R_{gb1} \\ C_{gb2} = K_C \cdot C_{gb1} \end{cases} \quad (3)$$

$$\text{where } K_R = 2 \cdot \left( \frac{S_1}{S_2} \right) \cdot \left( \frac{h_2}{h_1} \right) \text{ and } K_C = \frac{1}{2} \cdot \left( \frac{S_2}{S_1} \right) \cdot \left( \frac{h_1}{h_2} \right).$$

$S_2$  is the area below the half-turn and  $S_1$  the area of electrode disk,  $h_2$  is the height of the ferrite between the half-turn and ground plane and  $h_1$  the height between the electrode disks. Factors 2 and 1/2 in the expression of  $K_R$  and  $K_C$  stand for the fact that resistances and capacitances are equally distributed at each end of the half-turn.

Calculation of section  $S_2$  is done with the following expressions:

$$\begin{cases} S_2 = w \cdot l_i \\ l_i = \frac{1}{2} \cdot \pi \cdot [2 \cdot R_i + i \cdot w + (i-1) \cdot s] \end{cases} \quad (4)$$

$R_i$  is the inner radius of the spiral coil and  $l_i$  the mean length of each half-turn with  $i = 1$  to  $2n$ .

### Inter-turns impedances

The calculation of the inter-half-turn parameters is not quite easy. The co-planar electrodes of the tested sample have to be transformed into parallel plate electrodes by using the theory of conformal transformations developed in [15] [16]. New constants are derived from the transformation as in Equation (5).

$$K'_R = \frac{2 \cdot K(k)}{K(k')} \text{ and } K'_C = \frac{K(k')}{2 \cdot K(k)} \quad (5)$$

where  $K(k)$  is the complete integral of first kind with modulus  $k$ , and  $K(k')$  is the complete integral of the first kind taken in the complementary modulus  $k'$ .

The modulus  $k$  is given by the following expression:

$$\begin{cases} k = \frac{\tanh\left[\frac{\pi \cdot s}{4 \cdot h}\right]}{\tanh\left[\frac{\pi \cdot (w + 0.5 \cdot s)}{2 \cdot h}\right]} \\ k' = \sqrt{1 - k^2} \end{cases} \quad (6)$$

Using all these constants the parameters  $R_{g2}$ ,  $R_{gb2}$  and  $C_{gb2}$  of inter-half-turn are given by:

$$\begin{cases} C_{gb2} = \frac{1}{2} \cdot \left[ C_{gb1} \cdot \frac{K(k'_2)}{K(k_2)} \cdot \frac{K(k_1)}{K(k'_1)} \cdot \frac{l_{2i}}{l_1} \right] \\ R_{g2} = 2 \cdot \left[ R_{gb1} \cdot \frac{K(k_2)}{K(k'_2)} \cdot \frac{K(k'_1)}{K(k_1)} \cdot \frac{l_{2i}}{l_1} \right] \\ R_{g2} = 2 \cdot \left[ R_{g1} \cdot \frac{K(k_2)}{K(k'_2)} \cdot \frac{K(k_1)}{K(k'_1)} \cdot \frac{l_{2i}}{l_1} \right] \end{cases} \quad (7)$$

where  $l_{2i}$  is the mean length of inter-half-turn and  $l_1$  the transversal length of the electrodes of the tested sample.

$$l_{2i} = \frac{1}{2} \cdot \pi \cdot [2 \cdot R_i + (i + 1) \cdot w + i \cdot s] \quad (8)$$

with  $i = 1$  to  $2(n - 1)$ .

All the parameters of the filter can be now computed.

## 5. Mn-Zn Ferrite Filter Behaviour

### 5.1. Mn-Zn Ferrite Induced Electrical Conduction Power Losses

First simulations were performed by using the following physical and electrical parameters reported in **Table 3**.

As expected, a large amount of power losses takes place in both ferrite substrate and inter-turns areas, justifying that the Mn-Zn ferrites have never been used as capacitors. As an illustration, the filter efficiency, excluding magnetic and eddy current losses, has been calculated versus output power in **Figure 7**. An increase in the output power leads to an increase in the filter efficiency, but this efficiency is no higher than 37% at 1 kW which is obviously unacceptable. Moreover, this power level is not consistent with the conductor section which is not enough to carry such a power.

**Table 3.** Geometrical sizes and electrical data taken for the LC-filter behaviour simulation.

Buck	Spiral	Ferrite
Frequency: 100 kHz	Number of turns: 9	Permeability: 1800
Duty cycle: 0.5	Internal radius: 5 mm	Permittivity: $6.5 \times 10^4$
Input voltage: 200 V	Track thickness: 0.2 mm	Thickness: 1 mm
Load: 10 to 40 $\Omega$	Track width: 1 mm	

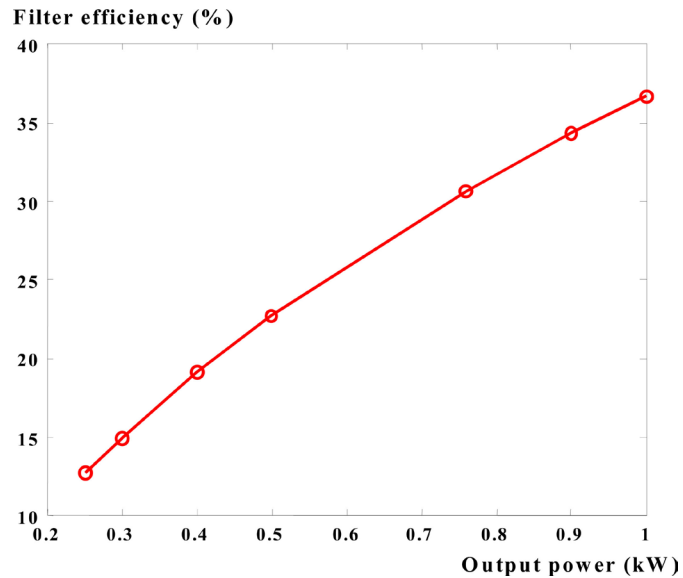


**Figure 7.** Simulation of the LC filter efficiency versus output Buck power ( $T = 20^{\circ}\text{C}$ ).

## 5.2. Power Losses Reduction

Power losses originating from the electrical conduction of the Mn-Zn substrate are located in the substrate bulk and in the inter-turns areas. The repartition of these losses has been estimated and revealed that these losses decrease versus inter-turns index, as indicated in **Table 4**. In our studied structure, electrical conduction losses are mainly located in the three firsts turns. Indeed this structure acts as a distributed low-pass filter. The higher the turn index, the lower the voltage ripple and consequently the lower the corresponding electrical conduction losses.

In order to reduce the electrical conduction losses, mainly located in the first turns, new simulations have been performed in which the inter-turns distances have been chosen to depend on the turn index. The inter-turns distance evolution law has been chosen linear and exponential successively in order to reduce the inter-turns losses. The chosen laws are detailed in **Table 5**.

The resulting losses have been reported in **Table 6**, showing that an exponential law is the better way to reduce the electrical conduction losses taking place in these areas of the substrates. Moreover, the voltage distribution in such a structure is not linear. The level of the inter-turns voltage depends on the inter-turns index: the lower the index, the higher the voltage level. Consequently, the exponential evolution chosen to reduce the inter-turns losses is interesting to increase the surface dielectric strength of the Mn-Zn substrates as well.

## 5.3. Multi-Materials LC Filter

In spite of the reducing in the power losses induced by the modification of the coil design, the resulting filter efficiency is no longer acceptable. New structures have therefore been proposed in **Figure 8** in order to increase this efficiency. Structure 1 is the initial structure which has been rejected. In structure 2, two

**Table 4.** Electrical conduction losses (% of the total electrical conduction losses) vs inter-turn index (three first turns – output Buck power = 1 kW).

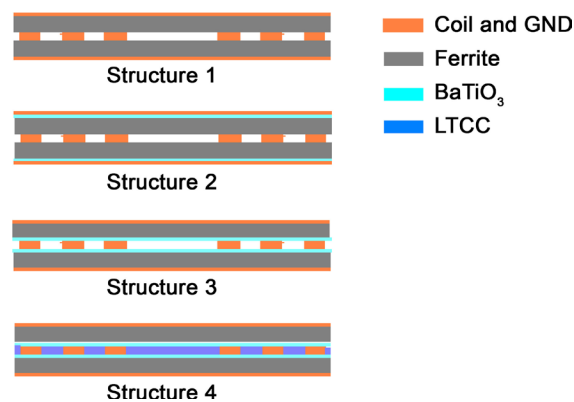
Turn index	1	2	3
Substrate losses (%)	77	8.5	1.3
Inter-turn losses (%)	11	1.4	0.2

**Table 5.** Different inter-turn gap evolution laws (i = Turn Index).

	Inter-turn gaps law (mm)
Constant	1
Linear	$(23.5 - 2.5 \times i)/7$
Exponential	$3 \times \exp[-0.256 \times (i - 1)]$

**Table 6.** Filter efficiency vs inter-turn gap evolution law (output power = 1 kW).

Inter-turn gap evolution law	Filter efficiency (%)
Constant	37
Linear	59
Exponential	63

**Figure 8.** Different studied filter topology.

“blocking” layers have been added in between the Mn-Zn substrates and the ground plates. In structure 3, these blocking layers have been put in between the coil and the Mn-Zn substrates. These layers have to exhibit a sufficiently high permittivity (in order to keep the advantage of Mn-Zn) and also a higher resistivity. Among available materials exhibiting such characteristics, BaTiO<sub>3</sub> has been chosen. As already done with Mn-Zn, a dielectric characterisation has been performed. The most suitable electrical model able to describe the experimental behaviour of BaTiO<sub>3</sub> is the same as those obtained with our Mn-Zn samples. The results obtained with a 130 μm-thick commercial (standard) BaTiO<sub>3</sub> film has been reported in **Table 7**.

In structure 3, the air gap between the two Mn-Zn substrates has been increased (+200 μm = BaTiO<sub>3</sub>), leading to a decrease in the corresponding induc-

tance  $L$ , and thus in the product  $LC$ .

Consequently, a complementary ferromagnetic material has been used to reduce this induced inconvenient. A low temperature co-firing ferrite tape (ferrite powder in organic matrix-LTCC-ESL 40012) has been chosen first of all for its interesting physical properties and secondly because it may be easily adapted to our complex structure (tapes which may be easily cut and hot-pressed to obtain the desired design and thickness). Physical data and the fitting parameters obtained on a 280  $\mu\text{m}$ -thick sample have been reported in **Table 8**. The equivalent electrical model of this tape is the same as Mn-Zn and  $\text{BaTiO}_3$  (**Figure 4(b)**).

Using successively structure 1 to 4, the filter efficiency has been estimated. In these simulations, an exponential inter-turns gaps law has been applied. The corresponding filter efficiencies are given in **Figure 9** (versus output power – duty cycle = 0.5) and **Figure 10** (versus duty cycle –  $I_{\text{load}} = 10 \text{ A}$ ).

All the structures show the same behaviour: the higher the output Buck power, the higher the corresponding efficiency.

**Table 7.** Fitting parameters of standard  $\text{BaTiO}_3$  AT  $T = 20^\circ\text{C}$  (frequency range: 10 Hz - 1 MHz).

$R_g (\Omega)$	$R_{gb} (\text{M}\Omega)$	$C_{gb} (\text{nF})$
116	3.8	24

**Table 8.** Datasheets and fitting parameters of the chosen magnetic tape at  $T = 20^\circ\text{C}$  (frequency range: 10 Hz - 1 MHz).

$T_C$	$\mu_r (F = 100 \text{ kHz})$	$R_g (\Omega)$	$R_{gb} (\Omega)$	$C_{gb} (\text{nF})$
$350^\circ$	450	12	$1.6 \times 10^{10}$	22

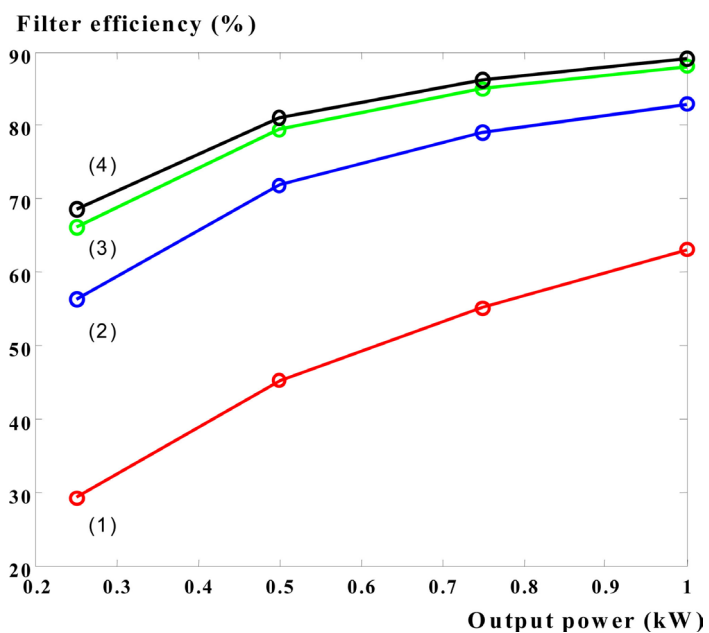


**Figure 9.** Simulation of the LC filter efficiency versus output Buck power (Structures 1 to 4 of **Figure 9**— $T = 20^\circ\text{C}$ —electrical data of **Table 2**).

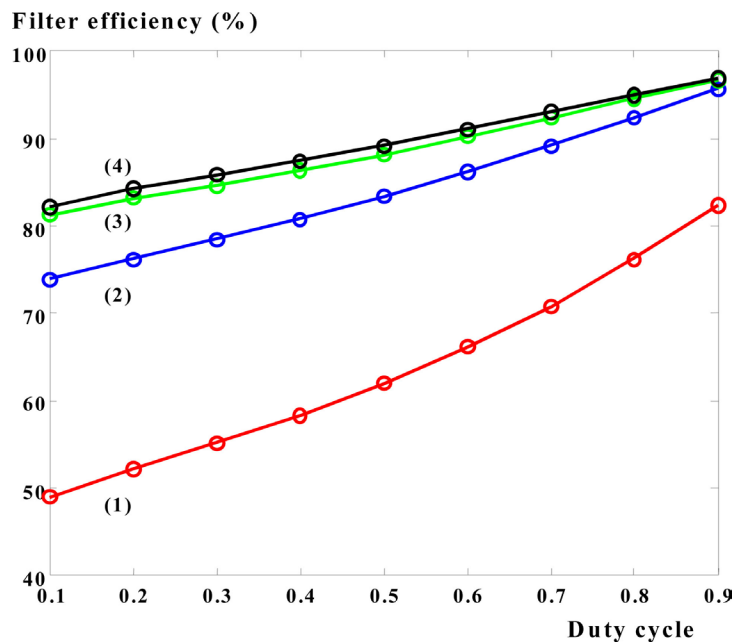


**Figure 10.** Simulation of the LC filter efficiency versus duty cycle (Structures 1 to 4 of **Figure 9**— $T = 20^\circ\text{C}$ —electrical data of **Table 2**— $I_{\text{load}} = 10\text{ A}$ ).

The goal of the  $\text{BaTiO}_3$  layers is to strongly reduce the power losses in Mn-Zn substrates in both volume and also inter-turns areas. In structure 2, only volume losses are reduced, while in structure 3 both volume and inter-turns losses are reduced, justifying that the structure 3 has a better efficiency (close to 90% at 1 kW – duty-cycle = 0.5).

As shown in this simulation, the losses reduction provided by the magnetic LTCC is not as high as expected. Moreover, keeping the air gap free may allow a complementary use of this gap. As an example, if the cooling of the DC converter is obtained by the use of a cooling fluid, this fluid may be injected in this gap to extract the heat produced by the filter.

As already mentioned, the spiral conductor is not, whatever the chosen structure, sufficient to carry 1 kW from the power supply to the load. New simulations have to be performed, using a suitable conductor cross section.

#### 5.4. New Dimensioning of the Studied Filter

By using a 200 V power supply, carrying 3 kW leads to a spiral conductor of  $3\text{ mm}^2$  (taking  $5\text{ A/mm}^2$ ). New simulations have been performed with this new conductor sizes. In **Figure 11** and **Figure 12**, the filter efficiency has been drawn versus output power (duty cycle = 0.5) and duty cycle ( $I_{\text{load}} = 15\text{ A}$ ). The filter using standard Mn-Zn and  $\text{BaTiO}_3$  ceramics (those characterized in this study) exhibits, as expected, satisfactory results. Nevertheless, an increase in the filter efficiency may be achieved by using ‘optimized’ ceramic materials (*i.e.*: low loss  $\text{BaTiO}_3$  [16] and Mn-Zn [17], same magnetic LTCC).

Electrical characteristics of such LC filters have been reported in **Table 9**. In the conventional filters, the value of L corresponds to the total inductance of our

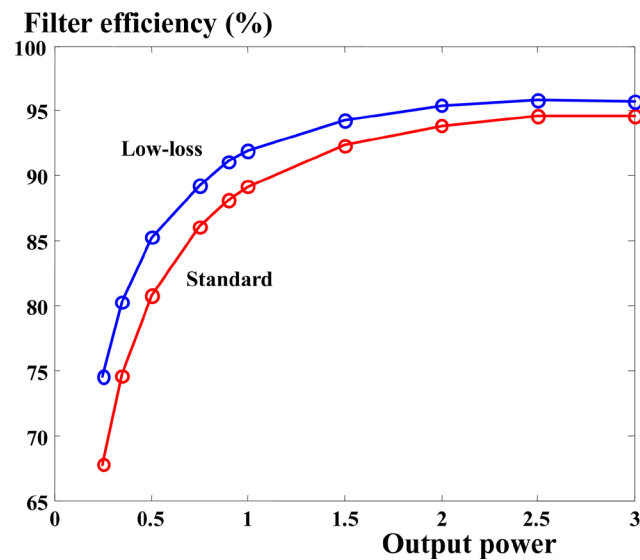


**Figure 11.** Simulation of the optimized LC filter efficiency versus output Buck power (duty cycle: 0.5), ( $T = 20^\circ\text{C}$ —electrical data of [Table 2](#)).

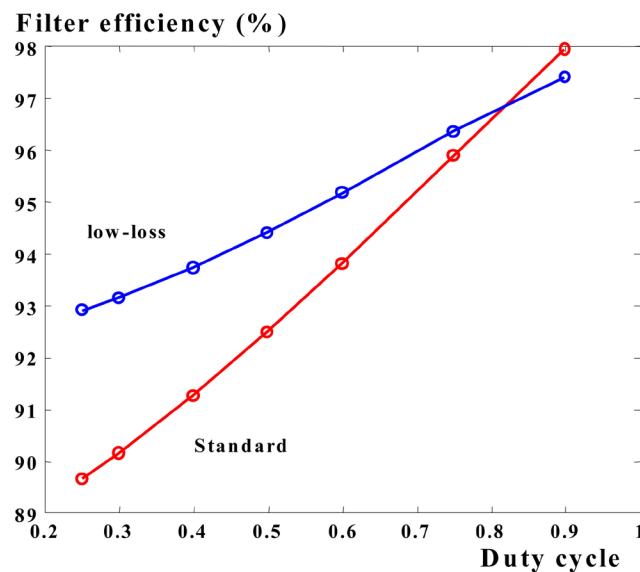


**Figure 12.** Simulation of the optimized LC filter efficiency versus duty cycle ( $T = 20^\circ\text{C}$ —electrical data of [Table 2](#)— $I_{\text{load}} = 15\text{ A}$ ).

**Table 9.** Electrical characteristics of our studied filter vs conventional structures.

	$F_c$ (-3 dB) (kHz)	Slope (dB/decade)	Attenuation at 100 kHz (dB)	Size ( $\text{cm}^3$ )	Weight (g)
LC filter using an air inductor and a plastic capacitor	43	-40	-4.87	186	431
LC filter using a Mn-Zn inductor and a plastic capacitor	43	-40	-4.87	25.5	180
Our LC planar studied filter	45	-180	-3.7	14.7	81
Optimized filter with low loss ceramics materials	33	-180	-11.5	14.7	81

filter while C to the total capacitance. As clearly shown in this table, our proposed LC filter is less heavy and bulky as conventional LC structures using discrete L and C components.

New optimizations are actually in progress to provide LC planar filters with lower cut-off frequencies in order to be used in DC-DC converters working at 10 - 20 kHz.

## 6. Conclusion

Mn-Zn ceramic substrates have been used in this work for both their high permeability and permittivity. Already largely used as core material, the goal of this study was to show that Mn-Zn may also be used as a capacitor in a DC-DC power converter integrated LC filter. The topology of this power filter is mainly composed of a circular coil between two Mn-Zn substrates. In order to reduce the Mn-Zn induced conduction power losses, the use of a blocking layer, such as BaTiO<sub>3</sub>, has been proposed. Modelling and simulation were used to estimate the filter electrical characteristics. Results have shown that a combination of Mn-Zn and BaTiO<sub>3</sub> ceramics materials allows the conception of power LC filters (a few kW) with a satisfactory efficiency. Future investigations are focused on the optimization of the filter design and the use of new synthesized materials in order to increase this efficiency.

## Acknowledgements

The authors would like to thank T. LEBEY for his useful discussions.

## References

- [1] Nhat Nguyen, M. and Meyer, R.G. (1990) Si IC-Compatible Inductors and LC filters. *IEEE Journal of Solid-State Circuits*, **25**, 1028-1031.  
<https://doi.org/10.1109/4.58301>
- [2] Artillan, P., Brunet, M., Bourrier, D., Laur, J.P., Mauran, N., Bary, L., Dilhan, M., Estibals, B., Alonso, C. and Sanchez, J.L. (2010) Integrated LC Filter on Silicon for DC-DC Converter Applications. *IEEE Transactions on Power Electronics*, **26**, 2319-2325.  
<https://doi.org/10.1109/TPEL.2010.2102776>
- [3] Coulibaly, S., Loum, G. and Diby, K.A. (2015) Design of Integrated LC Filter Using Multilayer Flexible Ferrite Sheets. *IOSR Journal of Electrical and Electronics Engineering*, **10**, 35-43.
- [4] Prieto, M.J., *et al.* (2002) Design and Analysis of Thick-Film Integrated Inductors for Power Converters. *IEEE Transactions on Industry Applications*, **38**, 543-552.  
<https://doi.org/10.1109/28.993177>
- [5] Sato, T., Hasegawa, M., Mizoguchi, T. and Sahashi, M. (1991) Study of High Power Planar Inductor. *IEEE Transactions on Magnetic*, **27**, 5277-5279.  
<https://doi.org/10.1109/20.278812>
- [6] Katayama, Y., Sugahara, S., Nakazawa, H. and Edo, M. (2000) High-Power-Density MHz Switching Monolithic DC-DC Converter with Thin-Film Inductor. *IEEE Power Electronics Specialists Conference*, **3**, 1485-1490.  
<https://doi.org/10.1109/PESC.2000.880526>

- 
- [7] Kawabe, K., Koyama, H. and Shirae, K. (1984) Planar Inductor. *IEEE Transactions on Magnetics*, **20**, 1804-1806. <https://doi.org/10.1109/TMAG.1984.1063271>
- [8] Kowase, I., Sato, T. and Yamasawa, K. (2005) A Planar Inductor Using Mn-Zn Ferrite/Polyimide Composite Thick Film for Low-Voltage, Large-Current DC-DC Converter. *IEEE Transactions on Magnetics*, **41**, 3991-3993. <https://doi.org/10.1109/TMAG.2005.855164>
- [9] Drogenik, M., Znidarsic, A. and Zajc, I. (1997) Highly Resistive Grain Boundaries in Doped Mn-Zn Ferrites for High Frequency Power Supply. *Journal of Applied Physics*, **82**, 333-340. <https://doi.org/10.1063/1.365817>
- [10] Nien, H.H., Liang, T.J., Huang, C.K., Changchien, S.K. and Shieh, H.W. (2006) Implementation of Low Loss Mn-Zn Ferrite Core for Power Electronics Applications. 2006 *IEEE Power India Conference*, New Delhi, 10-12 April 2006. <https://doi.org/10.1109/POWERI.2006.1632595>
- [11] Nien, H.H., Liang, T.J., Chen, J.F. and Changchien, S.K. (2007) Study of the Electrical and Magnetic Properties of MnZn Ferrite by Equivalent Electrical Elements. *Second International Conference on Innovative Computing Information and Control*, Kumamoto, 5-7 September 2007.
- [12] Nishiyama, H. and Nakamura, M. (1990) Capacitance of a Strip Capacitor. *IEEE Transactions on Components, Hybrids, and Manufacturing Technology*, **13**, 417-420. <https://doi.org/10.1109/33.56178>
- [13] Tang, C.-C., Wu, C.-H. and Liu, S.-I. (2002) Miniature 3-D Inductors in Standard CMOS Process. *IEEE Journal of Solid-State Circuits*, **37**, 471-480. <https://doi.org/10.1109/4.991385>
- [14] 2004 COMSOL FEMLAB Electromagnetic Module Reference Manual Version 3.0.
- [15] Gevorgian, S., Berg, H., Jacobson, H. and Lewin, T. (2003) Basic Parameters of Coplanar-Strip Waveguides on Multilayer Dielectric/Semiconductor Substrate, Part 1: High Permittivity Superstrates. *IEEE Microwave Magazine*, **4**, 60-70. <https://doi.org/10.1109/MMW.2003.1201599>
- [16] Zhao, L. (2004) Generalized frequency Plane Model of Integrated Electromagnetic Power Passives. Ph.D Dissertation, Virginia Polytechnic Institute and State University, Blacksburg.
- [17] Murty, S.R. (2003) Development of Low-Power Loss Mn-Zn Ferrites Using Microwave Sintering Method. *Bulletin of Materials Science*, **26**, 499-503. <https://doi.org/10.1007/BF02707347>